Influence of coincidence detection of a biphoton state through free-space atmospheric turbulence using a partially spatially coherent pump

Samukelisiwe Purity Phehlukwayo,[1] Marie Louise Umuhire,[1] Yaseera Ismail,[1,*] Stuti Joshi,[2,†] and Francesco Petruccione[1,3,‡]

[1]*Quantum Research Group, School of Chemistry and Physics, University of KwaZulu-Natal, Durban 4001, South Africa*
[2]*Department of Physics, Indian Institute of Technology Delhi, Hauz Khas, New Delhi 110016, India*
[3]*National Institute for Theoretical Physics (NITheP), KwaZulu-Natal, South Africa*

(Received 15 July 2020; accepted 2 September 2020; published 30 September 2020)

The development of a quantum network relies on the advances of hybrid systems which include ground-to-ground communication. However, the atmospheric turbulence of the environment poses a severe challenge to the optical quantum link. In this paper, we outline a theoretical and experimental investigation of the influence of atmospheric turbulence on the coincidence detection of the entangled photon pairs using a fully and partially spatially coherent pump beam. A spatial light modulator is encoded to mimic the atmospheric turbulence strength based on the Kolmogorov model of turbulence. The results show that the photon pairs generated using a partially spatially coherent pump are more robust towards varying atmospheric turbulence strengths than the photon pairs produced by a fully spatially coherent pump beam.

DOI: 10.1103/PhysRevA.102.033732

I. INTRODUCTION

Quantum communication is a promising physical process of upholding the security of information. It is considered the most secure method of data transfer, based on the encoding of single photons that are transmitted across fiber or a free-space link, which includes ground- and satellite-based communication [1–6]. At the core of the development of quantum technology is the phenomenon of entanglement. In photons, for example, entanglement may be encoded within all accessible degrees of freedom, such as the polarization, spatial, and spectral properties [7–9]. The generation (and distribution) of entanglement between photons generally forms the basis of modern quantum communication protocols.

Free-space quantum communication, in the spatial regime, is severely hindered by the influence of atmospheric turbulence. Turbulence is known to destroy the entanglement with spatial modes [10–13]. In the case of spatial modes, the decay of entanglement for the evolution of a qubit pair in turbulence has been studied both theoretically and experimentally [10–13]. Transmitting entangled photons, generated through spatial modes, through a free-space quantum channel results in the spatial modes being affected by the atmospheric turbulence, which reduces the probability of detection. Furthermore, the imposed scattering among spatial modes leads to a loss of entanglement in the final state measured in a specified subspace. Recently, it has also been shown that the turbulence also influences the detection scheme of polarization-based entanglement [14].

Besides quantum information science, entanglement has also found applications in numerous research areas such as optical imaging [15], ghost imaging [16,17], subwavelength interference, and microscopy [18]. These studies pointed out that the propagation of a two-photon entangled wave packet is equivalent to the propagation of the pump [19,20]. All of the studies mentioned above have been carried out by considering the pump to be fully spatially coherent. In some applications, partially spatially coherent beams are found to portray advantages over fully spatially coherent beams. Theoretical studies have shown the transfer of the angular profile [21] and spatial coherence of the pump into the twin-photon fields [22]. The experimental demonstrations of these studies confirm the effect of pump spatial coherence on the polarization-entangled [23] spatial coherence and entanglement properties of the down-converted field [24]. Entangled photons generated using a partially coherent pump are more robust to atmospheric turbulence than the entangled photons generated using a fully spatially coherent pump [25]. The generation of entangled photons using a partially coherent pump beam provides a flexible way to control entanglement between twin photons by the pump parameters.

In the present work, a theoretical and experimental study is carried out to investigate the influence of atmospheric turbulence on the coincidence between signal and idler photon pairs of a biphoton state. Our study is based on using a spatial light modulator encoded with a Kolmogorov model of turbulence [26,27] to mimic such effects. It is observed that the coincidence counts decrease as the atmospheric turbulence strength increases for different propagation distances. The observations show that the coincidence counts between the signal-idler photons generated using a partially spatially coherent pump beam (PSCPB) are less affected by the atmospheric turbulence than the coincidence counts between

*Ismaily@ukzn.ac.za
†stuti13@physics.iitd.ac.in
‡petruccione@ukzn.ac.za

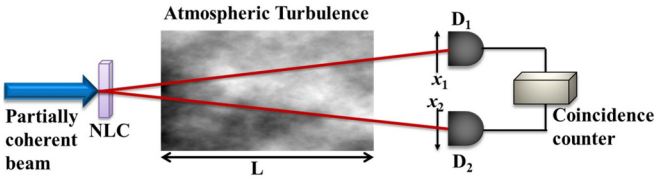

FIG. 1. Schematic to study the effect of atmospheric turbulence on entangled photons generated using a partially spatially coherent pump beam.

signal-idler photons generated using a fully spatially coherent pump beam (FSCPB). Here we provide experimental verification of the propagation of the entangled photons generated using a partially spatially coherent pump through varying atmospheric turbulence strengths. The present work shows the robustness of down-converted photons, generated using PSCPB, towards varying atmospheric turbulence strength, which would be useful in the practical design of entangled-photon-based free-space quantum communication systems.

II. THEORETICAL BACKGROUND

Free-space quantum communication entails the transfer of the generated single photons across a quantum channel, which can vary in atmospheric turbulence and propagation distance. The generic scenario to study the influences of atmospheric turbulence on the entangled photons generated using a PSCPB is shown in Fig. 1. The partially spatially coherent (PSC) pump interacts with a nonlinear crystal, responsible for spontaneous parametric down conversion (SPDC), and generates entangled photons according to the laws of conservation of energy and momentum [28]. This implies that a photon from a pump beam produces a single-photon pair known as a signal and an idler. The generated photons reach the detectors D_1 (positioned at x_1) and D_2 (positioned at x_2) after propagating a distance z through atmospheric turbulence, which represents the quantum link. Throughout the manuscript, p, s, and i refer to pump, signal, and idler, respectively. The biphoton state of the signal and idler $|\psi(x_1, x_2)\rangle$ at the detectors plane is given by [25,29]

$$|\psi(x_1, x_2)\rangle = \iint dq_s dq_i \eta(q_s, q_i) a^{\dagger}_{q_s} a^{\dagger}_{q_i} |0, 0\rangle, \tag{1}$$

where $|0, 0\rangle$ is the vacuum state, q_s and q_i refer to the transverse momentum of the signal and idler, respectively, at the crystal plane, and $a^{\dagger}_{q_s}$ and $a^{\dagger}_{q_i}$ are the creation operators of the signal and idler, respectively. We have assumed that the pump, signal, and idler are monochromatic and degenerate. The phase-matching function $\eta(q_s, q_i)$ is expressed as [29]

$$\eta(q_s, q_i) = \int dq_p V_p(q_p) \zeta(q_s, q_i) \delta(q_p - q_s - q_i), \tag{2}$$

where

$$\zeta(q_s, q_i) = \mathrm{sinc}\Big(\frac{\Delta q L}{2}\Big) \exp\Big(-\frac{i \Delta q L}{2}\Big), \tag{3}$$

with

$$\Delta q = \frac{q_p^2}{2k_p} - \frac{q_s^2}{2k_s} - \frac{q_i^2}{2k_i},$$

and $V_p(q_p)$ represents the pump field with transverse momentum coordinate q_p. L is the length of the nonlinear crystal, and k_p, k_s, and k_i refer to the wave vectors of the pump, signal, and idler, respectively.

At the detectors plane, D_1 and D_2, the positive component of the electric fields of the signal $[E_s^+(x_1, t)]$ and the idler $[E_i^+(x_2, t)]$ can be expressed in terms of annihilation operators as [29]

$$E_s^+(x_1, t) = \int dq_s H_s(x_1, q_s) \exp(-i\omega_s t) a^-_{q_s}, \tag{4}$$

$$E_i^+(x_2, t) = \int dq_i H_i(x_2, q_i) \exp(-i\omega_i t) a^-_{q_i}, \tag{5}$$

where $H_s(x_1, q_s)$ and $H_i(x_2, q_i)$ are the transfer functions of the signal and idler from the crystal plane to the detector plane, and ω_s and ω_i are the angular frequencies of the signal and the idler, respectively.

The coincidence count rate $R(x_1, x_2)$ between the signal and the idler can be calculated as [21]

$$R(x_1, x_2) = \langle \psi | E_s^-(x_1) E_i^-(x_2) E_i^+(x_2) E_s^+(x_1) | \psi \rangle. \tag{6}$$

By substituting Eqs. (1)–(5) into Eq. (6), and considering the pump to be PSC, the coincidence count rate can be written as

$$\begin{aligned} R(x_1, x_2) = \iiiint & dq_s' dq_i' dq_s dq_i \langle V_p^*(q_p') V_p(q_p) \rangle \\ & \times \eta^*(q_s', q_i') \eta(q_s, q_i) \\ & \times H_s^*(x_1, q_s') H_i^*(x_2, q_i') H_s(x_1, q_s) H_i(x_2, q_i). \end{aligned} \tag{7}$$

Equation (7) can also be written in terms of position coordinates of the signal and idler as

$$\begin{aligned} R(x_1, x_2) = \iiiint & d\rho_s d\rho_i d\rho_s' d\rho_i' W(\rho_s, \rho_i; \rho_s', \rho_i') \\ & \times h_s(x_1, \rho_s) h_i(x_2, \rho_i) h_s^*(x_1, \rho_s') h_i^*(x_2, \rho_i'), \end{aligned} \tag{8}$$

where $h_j(x_k, \rho_j)$ is the spatial inverse Fourier transform of $H_j(x_k, q_j)$; $j = s, i$ and $k = s, i$. Here, ρ_s and ρ_i are the spatial coordinates of the signal and idler, respectively, and $W(\rho_s, \rho_i; \rho_s', \rho_i')$ defines the two-photon cross-correlation function, which can be expressed in terms of the correlation between two spatial points (x_0 and x) of the pump and is given by

$$\begin{aligned} W(\rho_s, \rho_i; \rho_s', \rho_i') = \iint & dx dx_0 \langle V_p(x) V_p^*(x_0) \rangle \\ & \Lambda(\rho_s + \rho_i) \Lambda^*(\rho_s' + \rho_i'), \end{aligned} \tag{9}$$

with

$$x = \frac{\rho_s' + \rho_i'}{2} \quad \text{and} \quad x_0 = \frac{\rho_s + \rho_i}{2},$$

where $V_p(x)$ is the inverse Fourier transform of $V_p(q_p)$ and $\Lambda(\rho_s + \rho_i)$ is the Fourier transform of $\zeta(q_s, q_i)$. $h_j(x_1, x)$ is expressed as [30]

$$h_j(x_1, x) = A_j \exp\Big[-\frac{ik_j}{2z}(x_1^2 + x^2 - 2x_1 x) + \phi_j(x_1, x)\Big], \tag{10}$$

where $A_j = \sqrt{-\frac{ik_j}{2z\pi}}$, $j = s$ and i, z is the propagation distance, and $\phi_j(x_1, x)$ is the phase turbulence due to the scattering

in the atmosphere. To study the influence of atmospheric turbulence experimentally, we have utilized a spatial light modulator encoded with the Kolmogorov model of turbulence. The atmospheric structure constant C_n^2 describes the strength of the atmospheric turbulence [26,27]. The lateral coherence length under the influence of turbulence is related to C_n^2 as $\alpha_j = (0.55C_n^2k_j^2z)^{-3/5}$, $j = s, i$ [31].

The atmospheric turbulence function of the signal and the idler is expressed as [31]

$$\langle \exp[\phi_j^*(x_1, x')\exp[\phi_j(x_2, x)]\rangle = \exp\left[-\frac{(x_1-x_2)^2+(x_1-x_2)(x'-x)+(x'-x)^2}{\alpha_j^2}\right]. \tag{11}$$

We considered the pump to be a Gaussian Schell model such that the spatial correlation between two transverse points x and x' in the pump is given by [23,32]

$$\langle V_p^*(x')V_p(x)\rangle = A_p \exp\left(-\frac{x^2+x'^2}{4\sigma^2}\right)\exp\left[-\frac{(x'-x)^2}{2\delta^2}\right], \tag{12}$$

where A_p is a constant, and σ and δ, respectively, represent the beam waist and spatial coherence length of the pump beam at the crystal plane.

Now, by substituting Eqs. (9)–(12) into Eq. (8) and considering the paraxial approximation, and using $\mathrm{sinc}(\Delta qL)\approx\exp(-\gamma\sqrt{|\Delta q|}^2L/2)$ with $\gamma = 0.455$ [22], the coincidence count rate $R(x_1, x_2)$ can be written as

$$\begin{aligned} R(x_1,x_2) = {} & \frac{4\pi k_p}{L(\gamma^2+1)}\left(\frac{k_p}{4\pi z}\right)^2 \iiiint d\rho_s d\rho_i d\rho_s' d\rho_i' \exp\left\{-\frac{[(\rho_s+\rho_i)^2+(\rho_s'+\rho_i')^2]}{16\sigma^2}\right\} \\ & \times \exp\left[-\frac{(\rho_s'+\rho_i'-\rho_s-\rho_i)^2}{8\delta^2}\right]\exp\left[\frac{ik_p}{4z}(\rho_s^2-\rho_s'^2-2x_1\rho_s+2x_1\rho_s')\right] \\ & \times \exp\left[\frac{ik_p}{4z}(\rho_i^2-\rho_i'^2-2x_2\rho_s+2x_2\rho_i'^2)\right] \\ & \times \exp\left[-\frac{(\rho_s-\rho_s')^2-(\rho_i-\rho_i')^2}{\alpha^2}\right]\exp\left[\frac{k(\rho_s-\rho_i)^2}{4L(i+\gamma)}+\frac{k(\rho_s'-\rho_i')^2}{4L(-i+\gamma)}\right]. \end{aligned} \tag{13}$$

Equation (13) describes the coincidence count rate between the signal-idler photon pairs. The simplified analytic solution to Eq. (13) is provided in the Appendix. The coincidence count rate depends on the pump beam parameters (σ and δ) and the strength of the atmospheric turbulence for different propagation distances. Equation (13) is used to study the influence of atmospheric turbulence on the signal-idler photon pairs. Figure 2 shows the influence of varying atmospheric turbulence strength on the coincidence counts between the signal-idler photons by considering the pump to be spatially fully coherent ($\delta = \infty$) for different propagation distances. Figures 3–5 depict the coincidence counts of the biphoton field produced using a partially spatially coherent pump of spatial coherence length $\delta = 0.0876$, $\delta = 0.0417$, and $\delta = 0.0253$ mm, respectively.

To mimic the propagation of single photons through a free-space optical quantum link, we emphasize the importance of the effects of varying atmospheric turbulence on entangled photons generated using the fully and partially coherent pump source. To achieve this, we have theoretically studied the detection of coincidence counts (normalized) with respect to varying atmospheric turbulence strength (C_n^2), which is plotted in Fig. 6 using Eq. (13). The free-space propagation distance is chosen to be $z = 20$ km. Figure 6 illustrates that for larger propagation distances, at $z = 20$ km, the coincidence counts remain constant with the variation of (C_n^2) for a partially coherent pump source. However, there is a sharp exponential decrease in coincidence counts with (C_n^2) for a fully coherent pump source. This is due to the transfer of the spatial coherence of the pump to the down-converted photons [22]. A less spatially correlated pump produces a less spatially correlated biphoton field. This infers that a less correlated field after passing through the turbulent atmosphere or any scattering media produces less speckles and therefore shows robustness against varying atmospheric turbulence strengths.

In the present research, the influence of atmospheric turbulence on the coincidence counts for a fully and partially spatially coherent pump source is thoroughly explored and is followed by the experimental verification.

III. EXPERIMENTAL DESCRIPTION

Atmospheric turbulence is a major challenge in free-space quantum communication. Mitigation of these influences is necessary, especially for long-distance quantum links specifically for encoding in the spatial regime. We exploit the effects of the spatial distribution of the Gaussian pump beam to generate photon pairs with a well-defined degree of entanglement by manipulating the transverse coherence length of the pump [24]. Figure 7 illustrates our experimental setup to demonstrate the influence of atmospheric turbulence on the coincidence counts between signal-idler photon pairs. A concatenated β-barium borate (BBO) was used to produce entangled photon pairs through a type-I SPDC process. The dotted region of the experimental setup was used to produce the partial spatial coherence of the pump beam. A diode laser lasing at a wavelength of 405 nm was used to illuminate a rotating ground glass diffuser (RGGD) by passing through lens

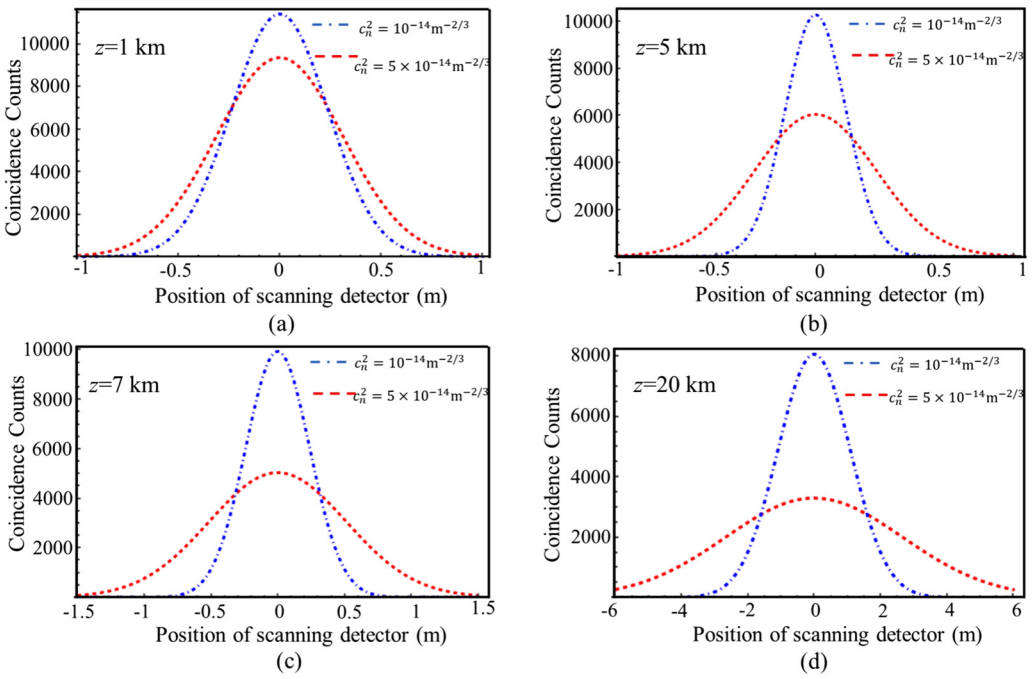

FIG. 2. Theoretical plots of coincidence counts as a function of the position of the scanning detector for different values of atmospheric turbulence strength when the pump is fully coherent ($\delta = \infty$). (a) $z = 1$ km, (b) $z = 5$ km, (c) $z = 7$ km, and (d) $z = 20$ km.

L_1 of focal length 50 mm. The pump beam was made partially spatially coherent at the BBO crystal by placing the RGGD and BBO crystal at the front and back focal plane of the lens L_2 ($f = 40$ mm), respectively [33]. Noncollinear ($\pm 3^\circ$ from the direction of the pump) degenerate entangled photon pairs of wavelength 810 nm were produced by pumping the BBO crystal with a partially spatially coherent pump beam. The generated photon pairs were passed through a Holoeye 1920×1080 spatial light modulator (SLM), which is a liquid-crystal device, utilized to mimic the atmospheric turbulence strength. The signal and idler photons were detected by single-photon detectors D_1 and D_2 through fiber couplers FC_1 and

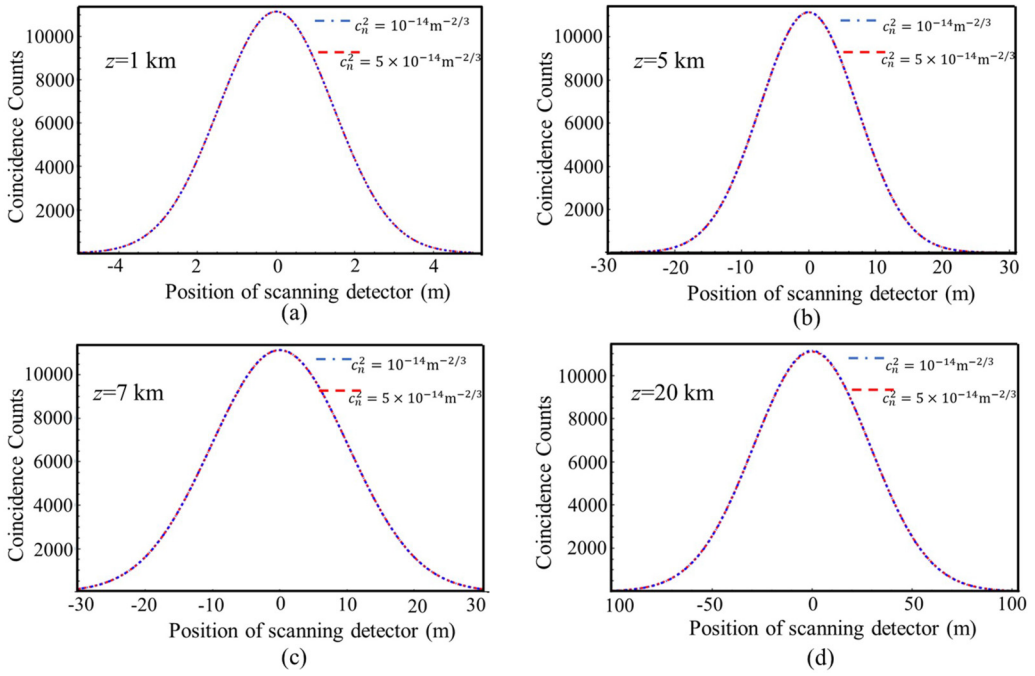

FIG. 3. Theoretical plots of coincidence counts as a function of the position of the scanning detector for different values of atmospheric turbulence strength when the pump is partially spatially coherent ($\delta = 0.0876$ mm). (a) $z = 1$ km, (b) $z = 5$ km, (c) $z = 7$ km, and (d) $z = 20$ km.

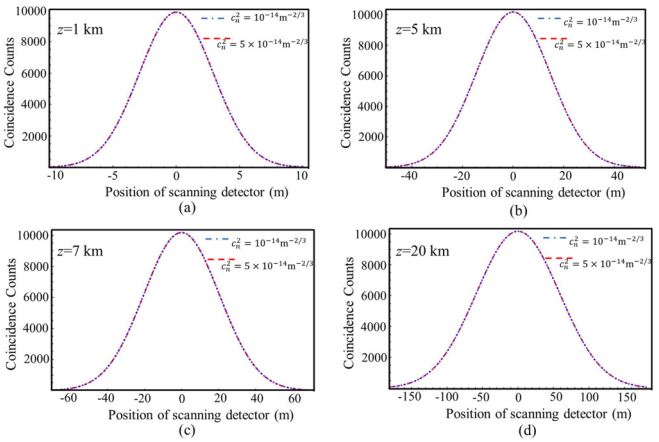

FIG. 4. Theoretical plots of coincidence counts as a function of the position of the scanning detector for different values of atmospheric turbulence strength when the pump is partially spatially coherent ($\delta = 0.0417$ mm). (a) $z = 1$ km, (b) $z = 5$ km, (c) $z = 7$ km and (d) $z = 20$ km.

FC_2, respectively. The transverse spatial distribution of the photon pairs can be observed by scanning the signal-idler detector in the transverse direction. In our experiment, the coincidence counts were recorded by fixing the signal detector at $x_1 = 0$ and scanning the idler detector in the transverse direction x_2.

IV. RESULTS AND DISCUSSION

In order to study the influence of atmospheric turbulence on the signal-idler photon pairs generated by the modulated pump beam, the strength of atmospheric turbulence was varied from $C_n^2 = 10^{-14}$ $m^{-2/3}$ (weak turbulence) to $C_n^2 = 5\times10^{-14}$ $m^{-2/3}$ (strong turbulence).

To demonstrate the influence of atmospheric turbulence on the coincidence detection experimentally, the SLM was encoded for weak and strong atmospheric turbulence strength

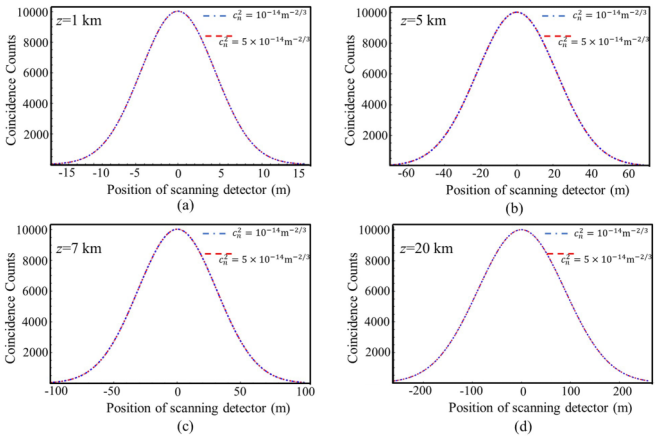

FIG. 5. Theoretical plots of coincidence counts as a function of the position of the scanning detector for different values of atmospheric turbulence strength when the pump is partially spatially coherent ($\delta = 0.0253$ mm). (a) $z = 1$ km, (b) $z = 5$ km, (c) $z = 7$ km and (d) $z = 20$ km.

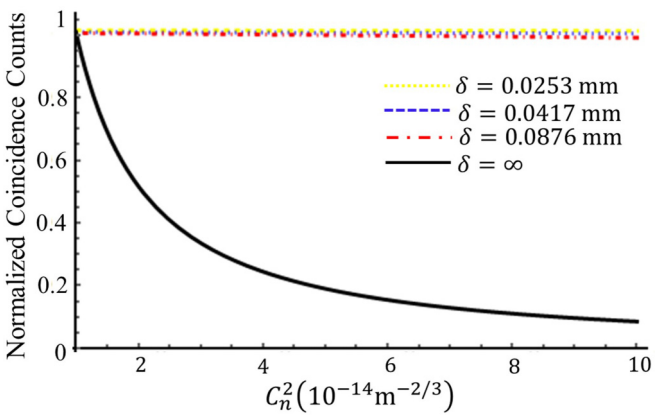

FIG. 6. Theoretical plots of normalized coincidence counts (at $x = y = 0$) as a function of C_n^2 at $z = 20$ km.

based on the Kolmogorov model [26,27]. Furthermore, the quantum link was varied in a number of distances ranging from 1–20 km. Initially, the fully spatially coherent pump beam was used to illuminate the BBO crystal in the absence of the diffuser system. The generated signal-idler photon pairs were passed through the SLM and detected in coincidence by fixing the signal at $x_1 = 0$ and scanning the idler in the transverse direction x_2. Figure 8 shows the experimental results depicting the influence of the atmospheric turbulence on the coincidence counts at different propagation distances. For a short distance ($z = 1$ km), a small decay in coincidence counts is observed when propagating through a stronger atmospheric

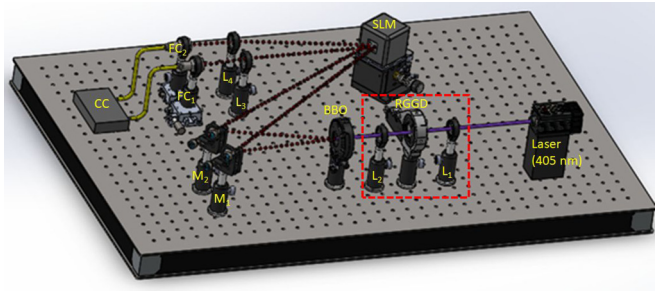

FIG. 7. Optical setup to verify the detection of coincidence counts for modulating partial spatial coherence in varying atmospheric turbulence. A fully coherent laser lasing at 405 nm was passed through a rotating ground glass diffuser (RGGD) and lens system (L_1 with a focal length 50 mm and L_2 with a focal length 40 mm) to produce the partial spatial coherence (dotted region). This field was passed through the type-I nonlinear crystal (BBO) where entangled single-photon pairs at 810 nm were generated through the process of spontaneous parametric down conversion. Mirrors M_1 and M_2 directed the photon pair towards a Holoeye 1920×1080 spatial light modulator (SLM). At this plane, the atmospheric turbulence was simulated for weak ($C_n^2 = 1 \times 10^{-14}$ $m^{-2/3}$) and strong ($C_n^2 = 5 \times 10^{-14}$ $m^{-2/3}$) turbulence with varying link distances of 1, 5, 7, and 20 km. Lenses L_3 and L_4, with focal lengths of 100 mm each, were used to focus the photons into the fiber couplers (FC_1 and FC_2), which were placed on translation stages for the scanning process. The single-photon pairs were detected by the coincidence counter (CC), which had embedded two single-photon avalanche detector modules D_1 and D_2.

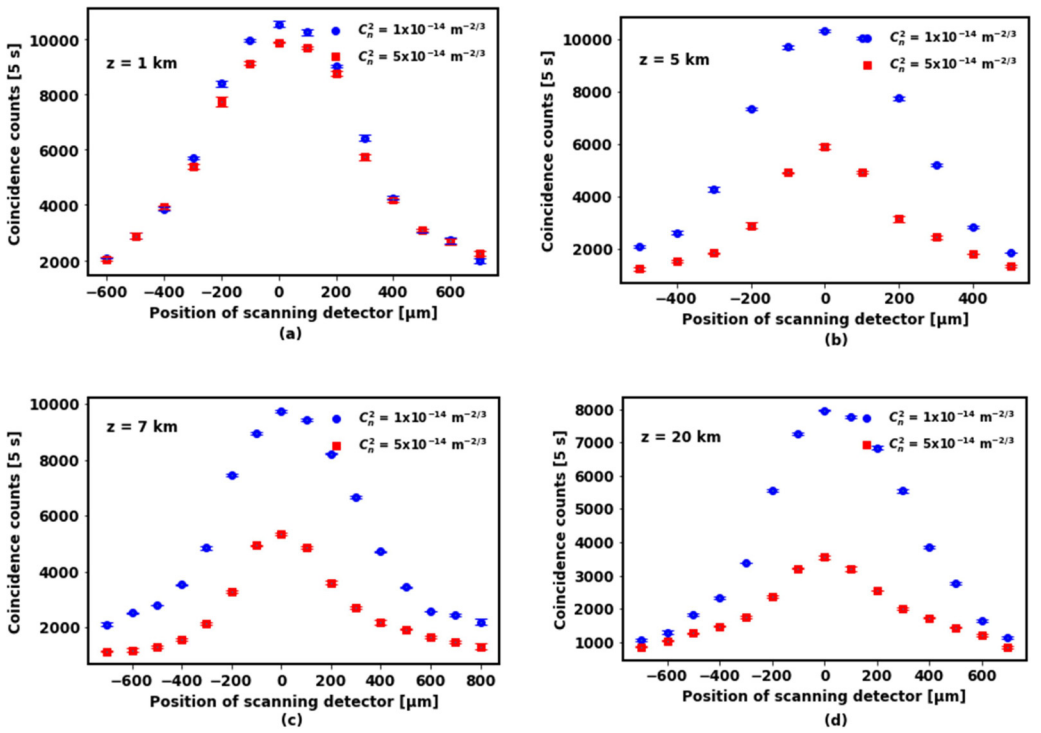

FIG. 8. Experimental plots of the effect of atmospheric turbulence on the coincidence counts when the pump is a fully spatially coherent ($\delta = \infty$) beam for different propagation distances. (a) $z = 1$ km, (b) $z = 5$ km, (c) $z = 7$ km and (d) $z = 20$ km.

turbulent strength ($C_n^2 = 5\times10^{-14}$ m$^{-2/3}$) compared to a weaker atmospheric turbulent strength ($C_n^2 = 10^{-14}$ m$^{-2/3}$), as shown in Figs. 2(a) and 8(a). This implies that when the propagation distance is less than 1 km, the effect of turbulence on the coincidence detection is small. As the photons propagate over longer distances, the difference in coincidence detection increases for the two values of C_n^2 (strong and weak), as shown in Figs. 2(b)–2(d) and Figs. 8(b)–8(d). The variation in maximum coincidence count detection for a fully coherent pump source at 1 km was 10% [Fig. 8(a)] between strong and weak turbulence. This variation reached 56% at 20 km [Fig. 8(d)]. Therefore, the detection of spatially generated photons becomes more difficult as they propagate through a longer distance in stronger turbulence. Next we made the pump to be partially spatially coherent at the crystal plane. The coherence length at the plane of the BBO crystal was calculated by $\delta = \frac{3.832\lambda f}{(2\pi d)}$ [33], where λ is the wavelength of the pump beam, f is the focal length of lens L_2, and d is the spot size at the diffuser plane. To obtain different values of the spatial coherence length, the spot size of the pump beam was varied at the diffuser plane by translating lens L_1.

The theoretical plots in Figs. 3–5 and the corresponding experimental results in Figs. 9–11 illustrate the influence of atmospheric turbulence on the coincidence detection, when the signal-idler photon pairs were produced by a partially spatially coherent pump ($\delta = 0.0876$, 0.0471, and 0.0253 mm, respectively), for different propagation distances. It is observed that the same coincidence detection was acquired for the two ranges of C_n^2 (strong and weak atmospheric turbulence) for short and longer propagation distances. This implies that the photon pairs produced with a low spatial coherence pump are less affected by the atmospheric turbulence strength. It was observed that for all of the aforementioned distances, the signal-idler photon pairs generated by the partially spatially coherent pump are less susceptible to atmospheric turbulence than the photon pairs produced with the fully spatially coherent pump.

To emphasize the advantage of the partial spatial coherence for varying atmospheric turbulence, the experimental observation of the normalized coincidence counts detected is further summarized in Fig. 12 for a propagation distance of 20 km. It was observed that for the fully coherent pump source (yellow solid curve), there is an exponential decay in the coincidence count detection as the atmospheric turbulence strength is increased. For the partially coherent pump source ($\delta = 0.0876$, 0.0417, 0.0253 mm), the coincidence count detection is almost constant (red dashed, blue dotted, and green dash-dotted curve, respectively). This complies with the theoretical observations in Fig. 6. By modifying the spatial coherence of the pump beam, we produce entangled photons which are considered weak measurements; however, even though this has implications on the strength of the entanglement [24], it does prove to be resistance to varying atmospheric turbulence. For a free-space quantum communication link, this can be circumvented by increasing the transmission time and hence sending more photons through the quantum channel to produce the secure key.

V. CONCLUSION

In conclusion, we have theoretically and experimentally demonstrated the influence of atmospheric turbulence on the coincidence detection of entangled photons produced by a fully and partially coherent pump source. It was suggested

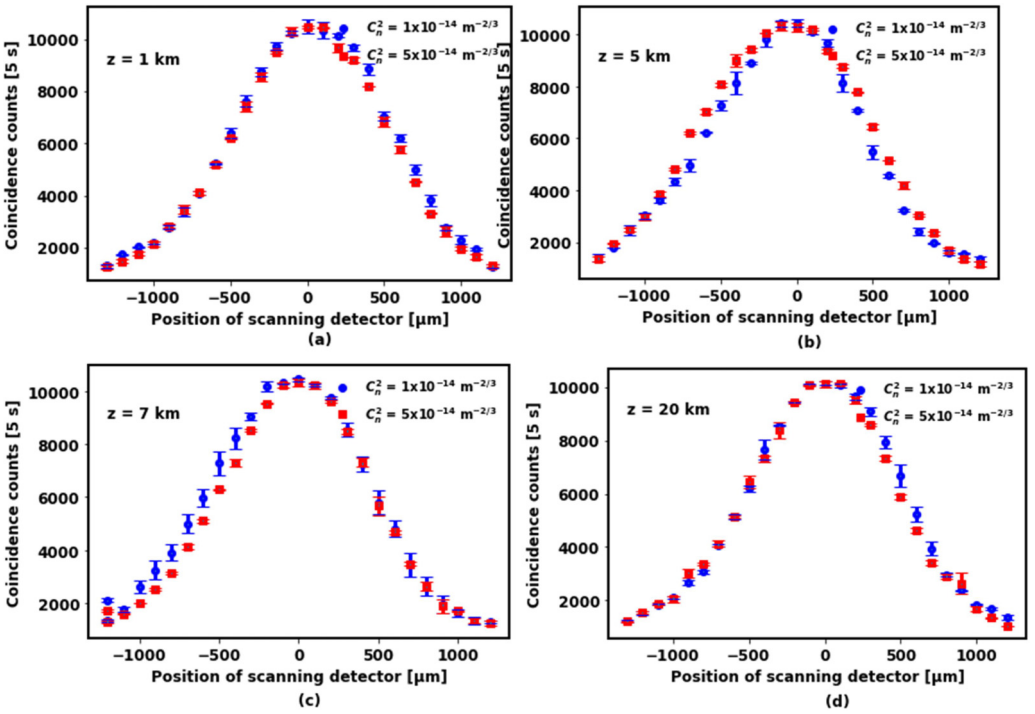

FIG. 9. Experimental plots of the effect of atmospheric turbulence on the coincidence counts when the pump is partially spatially coherent ($\delta = 0.0876$ mm) for varying propagation distances. (a) $z = 1$ km, (b) $z = 5$ km, (c) $z = 7$ km, and (d) $z = 20$ km.

by Zhang *et al.* that the study of varying the partial spatial coherence through atmospheric turbulence would provide interest for the application of quantum communication [34]. To simulate the free-space quantum link, a spatial light modulator encoded with the Kolmogorov model was used to mimic the atmospheric conditions. The RGGD was used in combination with a lens in a $2f$ geometry to produce the partially spatially coherent pump beam at the BBO crystal plane. It was found that the coincidence counts remained the same for weak and strong turbulence when the signal-idler photons pairs were generated using a partially spatially coherent pump for different propagation distances. However, there is

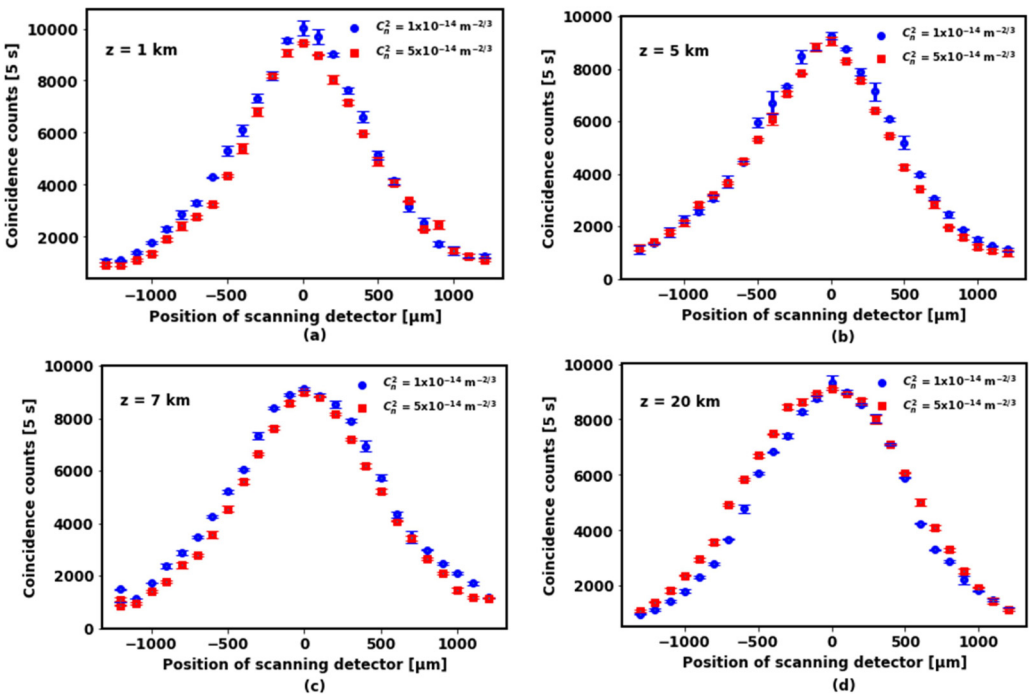

FIG. 10. Experimental plots of the effect of atmospheric turbulence on the coincidence counts when the pump is partially spatially coherent ($\delta = 0.0417$ mm) for varying propagation distances. (a) $z = 1$ km, (b) $z = 5$ km, (c) $z = 7$ km and (d) $z = 20$ km.

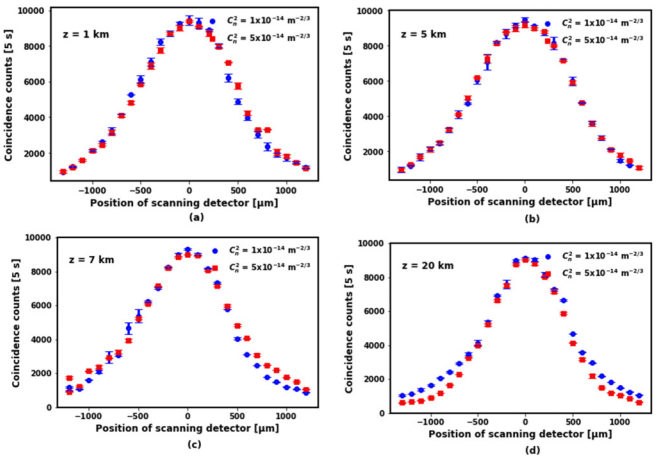

FIG. 11. Experimental plots of the effect of atmospheric turbulence on the coincidence counts when the pump is partially spatially coherent ($\delta = 0.0253$ mm) for varying propagation distances. (a) $z = 1$ km, (b) $z = 5$ km, (c) $z = 7$ km and (d) $z = 20$ km.

a decrease in coincidence counts for strong turbulence when entangled photons are produced with a fully spatially coherent pump beam. This implies that the entangled-photon pairs generated using a partially spatially coherent pump are more robust towards varying atmospheric turbulence strength than the entangled photons generated using a fully spatially coherent pump. Despite it being suggested that the partial spatial coherent pump has implications on the single-photon generation, there is a significant resilience toward atmospheric turbulence, especially for longer propagation distances. These results may find important applications in free-space quantum communication using spatially entangled photons.

ACKNOWLEDGMENTS

This work is based on research supported by the South African Research Chair Initiative of Department of Science and Technology and National Research Foundation as well as the Thuthuka grant. Opinions expressed and conclusions arrived at are those of the authors and are not necessarily to be attributed to the NRF. S.J. acknowledges financial support through the Indian Institute of Technology Delhi postdoctoral fellowship.

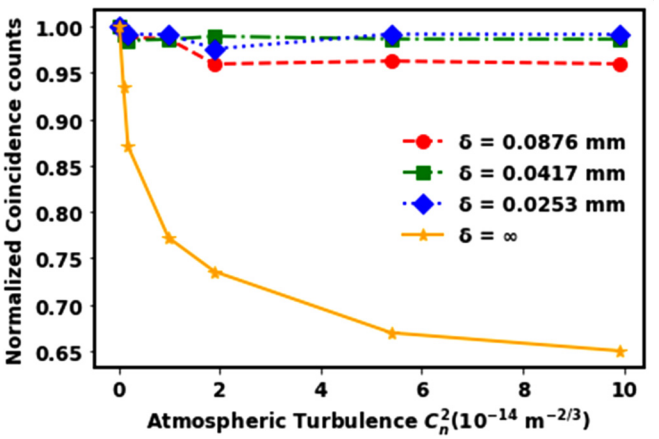

FIG. 12. Experimental plots of normalized coincidence counts (at $x = y = 0$) as a function of C_n^2 at $z = 20$ km for fully and partially coherent pump sources ($\delta = 0.0876, 0.0417, 0.0253$ mm).

APPENDIX

In this Appendix, we show the analytic solution to the detection of the coincidence counts, given by Eq. (13), by performing each of the integrals over different parameters, given as

$$
\begin{aligned}
&R(x_1, x_2) \\
&= A \exp\left(-\frac{k_p^2}{16M_1 z^2}\left[x_1^2 + \frac{A_1^2 x_1^2}{M_1 M_3} + \frac{x_2^2 M_1}{M_3} + \frac{2A_1 x_1 x_2}{M_3}\right]\right. \\
&\left. + \frac{k_p^2}{16M_4 z^2}\left[-1 - \frac{A_3^2 x_1^2}{4M_1^2} + \frac{A_3 x_1^2}{M_1} + \frac{A_4 x_1 x_2}{M_3} - \frac{A_4^2 x_2^2}{4M_3^2}\right]\right) \\
&\times \exp\left(\frac{A_4 k_p^2 x_1}{16 z^2 M_1 M_3 M_4}\left[A_1 x_1 - \frac{A_3 x_2}{2}\right.\right. \\
&\left.\left. + - \frac{A_1^2 x_1}{4M_1 M_3} - \frac{A_1 A_3 x_1}{2M_1} - \frac{A_1 x_2}{2M_3}\right]\right) \\
&\times \exp\left(\frac{1}{4M_5}\left[-\frac{ik_p x_2}{2z} + \frac{ik_p x_1}{16\delta^2 M_1 z} + \frac{iA_1 A_5 k_p x_1}{4M_1 M_3 z}\right]^2\right. \\
&\left. + \frac{iA_6 k_p}{4M_1 z}\left[\frac{A_1 A_4 x_1}{2M_1 M_3} + \frac{A_4 x_2}{2M_3} - x_1 + \frac{A_3 x_1}{2M_1}\right]\right),
\end{aligned}
$$

with

$$
\begin{aligned}
A &= \frac{4\pi k_p}{L\sqrt{\gamma^2 + 1}}\left(\frac{k_p}{4\pi z}\right)^2, \\
A_{1/2} &= -\frac{k_p}{4L(\pm i + \gamma)} + \frac{1}{8\delta^2} + \frac{1}{16\sigma^2}, \\
A_3 &= \frac{1}{4\delta^2} + \frac{2}{\alpha^2}, \\
M_{1/2} &= \mp\frac{ik_p}{4z} + \frac{k_p}{4L(\mp i + \gamma)} + \frac{1}{2}\left(\frac{1}{4\delta^2} + \frac{2}{\alpha^2}\right) + \frac{1}{16\sigma^2}, \\
M_3 &= M_1 - \frac{A_1^2}{M_1}, \\
A_4 &= \frac{A_1 A_3}{M_1} + \frac{1}{4\delta^2}, \\
A_5 &= A_3 + \frac{A_1}{4\delta^2 M_1}, \\
M_4 &= M_2 - \frac{A_3^2}{4M_1} - \frac{A_4^2}{4M_3}, \\
A_6 &= -2A_2 + \frac{A_4 A_5}{2M_3} + \frac{A_3 \alpha}{2M_1}, \\
M_5 &= M_2 - \frac{\alpha^2}{4M_1} - \frac{A_6^2}{4M_4} - \frac{A_5^2}{4M_3}.
\end{aligned}
$$

[1] R. Ursin, F. Tuefenbacher, T. Schmitt-Manderbach *et al.*, Nat. Phys. **3**, 481 (2007).

[2] J. Yin, J. G. Ren *et al.*, Nature (London) **488**, 185 (2012).

[3] J. Yin, Y. Cao, Y. H. Li, S. K. Liao, L. Zhang, J. G. Ren *et al.*, Science **356**, 1140 (2017).

[4] S. K. Liao, W. Q. Cai, W. Y. Liu *et al.* Nature (London) **549**, 43 (2017).

[5] P. Eraerds, N. Walenta, M. Legre, N. Gisin, and H. Zbinden, New J. Phys. **12**, 063027 (2010).

[6] Z. Q. Yin, Z. F. Han, W. Chen, F. X. Xu, Q. L. Xu, and G. C. Guo, Phys. Lett. **25**, 3547 (2008).

[7] J. Brendel, N. Gisin, W. Tittel, and H. Zbinden, Phys. Rev. Lett. **82**, 2594 (1999).

[8] P. G. Kwait, K. Mattle, H. Wienfurter, A. Zeilinger, A. V. Sergienko, and Y. Shih, Phys. Rev. Lett. **75**, 4337 (1995).

[9] J. C. Howell, R. S. Bennink, S. J. Bentley, and R. W. Boyd, Phys. Rev. Lett. **92**, 210403 (2004).

[10] A. A. Semenov and W. Vogel, Phys. Rev. A **81**, 023835 (2010).

[11] A. K. Jha, G. A. Tyler, and R. W. Boyd, Phys. Rev. A **81**, 053832 (2010).

[12] H. Avetisyan and C. H. Monken, Opt. Express **24**, 2318 (2016).

[13] Y. Zhang, S. Prabhakar, A. H. Ibrahim, F. S. Roux, A. Forbes, and T. Konrad, Phys. Rev. A **94**, 032310 (2016).

[14] Y. Ismail, S. Joshi, A. Forbes, and F. Petruccione, J. Opt. Soc. Am. B **34**, 1084 (2017).

[15] T. B. Pittman, Y. H. Shih, D. V. Strekalov, and A. V. Sergienko, Phys. Rev. A **52**, R3429 (1995).

[16] D. V. Strekalov, A. V. Sergienko, D. N. Klyshko, and Y. H. Shih, Phys. Rev. Lett. **74**, 3600 (1995).

[17] P. Zerom, K. W. C. Chan, J. C. Howell, and R. W. Boyd, Phys. Rev. A **84**, 061804(R) (2011).

[18] M. D'Angelo, M. V. Chekhova, and Y. Shih, Phys. Rev. Lett. **87**, 013602 (2001).

[19] A. Joobeur, B. E. A. Saleh, T. S. Larchuk, and M. C. Teich, Phys. Rev. A **53**, 4360 (1996).

[20] A. F. Abouraddy, B. E. Saleh, A. V. Sergienko, and M. C. Teich, JOSA B **19**, 1174 (2002).

[21] C. H. Monken, P. H. Souto Ribeiro, and S. Pádua, Phys. Rev. A **57**, 3123 (1998).

[22] A. K. Jha and R. W. Boyd, Phys. Rev. A **81**, 013828 (2010).

[23] Y. Ismail, S. Joshi, and F. Petruccione, Sci. Rep. **7**, 12091 (2017).

[24] H. Defienne and S. Gigan, Phys. Rev. A **99**, 053831 (2019).

[25] Y. Qiu and W. She, Appl. Phys. B **108**, 683 (2012).

[26] A. N. Kolmogorov, Dokl. Akad. Nauk SSSR **32**, 16 (1941).

[27] A. N. Kolmogorov, Dokl. Akad. Nauk SSSR **30**, 301 (1941).

[28] D. C. Burnham and D. L. Wienberg, Phys. Rev. Lett. **25**, 84 (1970).

[29] B. E. A. Saleh, A. F. Abouraddy, A. V. Sergienko, and M. C. Teich, Phys. Rev. A **62**, 043816 (2000).

[30] J. W. Goodman, *Introduction to Fourier Optics* (Roberts and Company Publishers, Greenwood Village, CO, 2005).

[31] S. C. H. Wang and M. A. Plonus, J. Opt. Soc. Am. A **69**, 1297 (1979).

[32] L. Mandel and E. Wolf, *Optical Coherence and Quantum Optics* (Cambridge University Press, Cambridge, 1995).

[33] J. T. Foley, J. Opt. Soc. Am. A **8**, 1099 (1991).

[34] W. Zhang, R. Flicker, E. Giese, L. Chen, and R. W. Boyd, Opt. Express **27**, 20745 (2019).